Article:
Lao, Y-F, Perera, AGU, Li, LH orcid.org/0000-0003-4998-7259 et al. (3 more authors) (2014) Tunable hot-carrier photodetection beyond the bandgap spectral limit. Nature Photonics, 8 (5). pp. 412-418. ISSN 1749-4885

https://doi.org/10.1038/nphoton.2014.80

Tunable hot-carrier photodetection beyond the band-gap spectral limit

Yan-Feng Lao[1], A. G. Unil Perera[1⋆], L. H. Li[2], S. P. Khanna[2], E. H. Linfield[2], and H. C. Liu[3]

[1]*Department of Physics and Astronomy, Georgia State University, Atlanta, GA 30303, USA*

[2]*School of Electronic and Electrical Engineering, University of Leeds, Leeds LS2 9JT, United Kingdom*

[3]*Key Laboratory of Artificial Structures and Quantum Control, Department of Physics, Shanghai Jiao Tong University, Shanghai 200240, China*

The spectral response of common optoelectronic photodetectors is restricted by a cut-off wavelength limit (λ_c) that is related to the activation energy (or band-gap) of the semiconductor structure (or material) ($\triangle$) through the relationship: $\lambda_c = hc/\triangle$. This spectral rule dominates device design and intrinsically limits the long wavelength response of a semiconductor photodetector. Here, we report a new, long wavelength photodetection principle based on a hot-cold hole energy transfer mechanism that overcomes this spectral limit. Hot carriers injected into a semiconductor structure interact with cold carriers and excite them to higher energy states. This enables a very long-wavelength infrared response. In our experiments, we observe a response up to 55 μm, which is tunable by varying the degree of hot-hole injection, for a GaAs/AlGaAs sample with $\triangle$ = 0.32 eV (equivalent to 3.9 μm in wavelength).

Dated: March 7, 2014

Recently, there has been increasing interest in using hot-carrier driven effects for photodetection. [1–4] Historically, the investigation of hot-carrier dynamics [5–7] has underpinned a broad range of studies into fundamental semiconductor physics and device design. The hot carriers, injected electrically or optically, typically relax through interactions with lattice vibrations, cold carriers and impurities. Of these processes, inelastic scattering with the lattice constitutes the major cooling path, and is predominantly accompanied by emission of optical phonons. [8–10] The excess energies of the hot carriers are thus ultimately converted into heat, which degrades the energy efficiency of devices. With sufficiently high energy above a threshold, hot carriers can initiate a carrier multiplication process. [11,12] This effect has been used for devices such as avalanche photodiodes to enhance optical gain. [13] Hot-carrier effects have also been used extensively for photodetection. [1–4] The principle is based on the transport of hot carriers under a built-in electric field, [1] or a hot-carrier induced temperature variation which either gives rise to a thermoelectric current [2,3] or alters the resistance of the device. [4] In contrast to these studies, however, interaction between hot and cold carriers, and the use of this interaction to realize novel device designs has received little attention. The significance of this approach is that it allows hot-carrier effects to be used for designing devices which operate principally based on cold carriers, enabling traditional semiconductor band-structure engineering technology to be used.

We report here a new concept for photodetection based on a hot-cold hole energy transfer mechanism. This enables a dramatic spectral extension, surpassing the standard limit set by the spectral rule $\lambda_c = hc/\Delta$, [14] where λ_c is the maximum wavelength limit and Δ is the activation energy of the optical transition during operation. This spectral extension is interpreted as a result

of energy transfer from injected hot holes to the cold holes in the absorber. The cold holes are therefore excited into higher energy states, and capable of responding to longer-wavelength infrared radiation than would be possible without the hot-hole injection. This idea also enables λ_c and Δ to be individually optimized in order to achieve targeted wavelengths for detection whilst simultaneously minimizing the detector noise and dark current. Moreover, as the hot carriers divert their energy to cold carriers rather than heating up the lattice, improvement in the energy efficiency of devices is expected.

Device structure and characterization

Semiconductor heterostructures based on p-type GaAs/$Al_xGa_{1-x}As$ were used to demonstrate this discovery. As shown in Fig. 1a, they consist of three p-type GaAs regions ($p = 1 \times 10^{19}$ cm^{-3}), i.e., an injector, absorber and collector (see Methods), for which the valence-band (VB) alignment is schematically plotted in Figs. 1b (equilibrium) and 1c (negative bias). The injector provides a hot-hole reservoir upon photoexcitation. Holes surmounting the barrier are "hot" because of their excess energies relative to the band edge of the absorber. [12]

The photoresponse shown in Fig. 1d was measured at 5.3 K (for details of the device structure, fabrication and characterization, see Methods and Supplementary Information I and II). The most striking fact is that, a very long-wavelength infrared (VLWIR) response is seen up to 55 μm, whilst the conventional limit is only 3.9 μm (shaded region) according to the internal work function (i.e., Δ) [15] of the absorber/constant barrier junction ($\Delta = 0.32$ eV, see Supplementary Information

II). The agreement between λ_c and Δ in terms of $\lambda_c = hc/\Delta$ is typically found to be good in a variety of detectors, [16,17] and has been used as a guideline to tune spectral response through varying Δ, [18] and to determine band offsets. [15] However, there is clearly no agreement for the observed VLWIR response in this case.

In general the observed VLWIR response could be due to a bolometric effect, [4] or an impurity-band/free-hole carrier [16,18] based response. Possible optical transitions contributing to photon absorption by the p-type GaAs absorber in the infrared range include the impurity band-to-valence band transition, [19] and intra-/inter-valence band transitions, [20] both of which are free-carrier type effects. Increasing the doping concentration shifts the absorption peak and broadens the absorption width, as a result of enhanced carrier scatterings, and the shifting/increasing of the Fermi level/free-carrier plasma frequency, respectively. [20,21] The absorber, though, has a major effect on the bolometric response and impurity-band absorption. By measuring a control sample (LH1002) which contains the same GaAs absorber as the samples SP1005 – 1007 (SP1005 – 1007 display a VLWIR response; see Fig. 1e), we can exclude these two mechanisms as a cause of the VLWIR response. LH1002 responds as expected, in accordance with the "$\lambda_c = hc/\Delta$" rule. Comparison of LH1002 (having a symmetric flat-barrier configuration; see Methods) with SP1005 – 1007 (asymmetric band alignment) indicates that the VLWIR response is critically dependent on the structure details. Additionally, the bolometric response, proportional to the temperature variation of the absorber upon photon absorption and the corresponding resistance change, monotonically increases with increasing bias. This effect contrasts with the strongly non-monotonically bias-dependent

VLWIR response, as shown in the calculated spectral weight (SW) (Figs. 2a and 2b), defined as

$$SW \propto \int_{\lambda_{\min}}^{\lambda_{\max}} \mathcal{R}(\lambda)\, d\lambda \tag{1}$$

where $\mathcal{R}(\lambda)$ is the spectral responsivity. The VLWIR response reaches a maximum at about -0.1 V. For these reasons, a bolometric effect cannot be considered to be contributing to the VLWIR response. Also, the impurity-band to valence-band optical transition can barely have any influence on the response, as the impurity band is actually merged with the VB [15,19] at $p = 1 \times 10^{19}$ cm^{-3}. Another possible doping-related effect is dopant-correlated potential fluctuations and the relevant tailing states at the band edge; however, absorbing photons with energies as high as the value Δ are required to excite holes in these band tailing states and allow them to escape over the barrier. Instead, here, we discuss a two-phase hot-hole mechanism to explain the VLWIR response: hot-cold hole energy transfer, and the response of high-energy cold holes to the VLWIR radiation. The dominant absorbing mechanism will then be based on the intra-band free-hole absorption. [15] It should be noted that the free-carrier based VLWIR response in this work differs markedly from the previous reported free-carrier response (see, for example, Ref. [17]) in which a small value of Δ is required.

Hot-cold carrier interactions

The short-wavelength portion of light from a Fourier transform infrared (FTIR) spectrometer (its power spectrum is shown in Fig. 1e), or more generally from an external optical excitation source (denoted as the "pump"), is essential to generate photoexcited hot holes and establish the VLWIR response. The pump-excited holes with energies higher than all of the barriers can be described by

a three-dimensional drift model, [22]

$$I_{ph}^{\text{pump}} = e \cdot v(F) \int_{\Delta}^{+\infty} N(\epsilon)\, d\epsilon \tag{2}$$

where I_{ph}^{pump} is the pump current. $N(\epsilon)$ is the concentration of holes with energy ϵ. [23] The electric field F is evaluated across the barrier regions. The drift velocity $v(F)$ is associated with an empirical fitting parameter – the mobility, [22] which is dependent upon both the doped GaAs absorber and undoped AlGaAs barrier. Despite its simplicity, Eq. 2 accounts for the current-voltage characteristics reasonably well in most devices. [22] Taking the derivative of I_{ph}^{pump} with respect to F gives

$$\frac{dI_{ph}^{\text{pump}}}{dF} = e \cdot \frac{dv(F)}{dF} \int_{\Delta}^{+\infty} N(\epsilon)\, d\epsilon - e \cdot v(F) \frac{d\Delta}{dF} \cdot N(\Delta) \tag{3}$$

in which $d\Delta/dF$ is mainly determined by the image-force barrier lowering [15] and tilting of the graded barrier by applied bias. In the high-field region, the first term of Eq. 3 vanishes since $v(F)$ approaches a constant saturation velocity. The energy distribution of holes is thus proportional to the differential I_{ph}^{pump}, which consists of photocarriers with different energies. I_{ph}^{pump} can be evaluated by using Eq. 1 or directly measured in experiment. As shown in Fig. 2c (top panel), the differential SW displays three distribution peaks at -0.12, -0.40 and 0.10 V, which were confirmed by photocurrent-voltage characteristics measured using different optical excitation sources (bottom panel of Fig. 2c). In terms of hot-carrier spectroscopy, [23,24] the occurrence of distribution peaks is a sign of a hot-cold carrier interaction which leads to the excitation of cold carriers into higher energy states. Studies [25] have shown that under a low applied bias the electric field is nonuniformly distributed, mainly across the graded barrier region. With increasing negative bias, the graded barrier is tilted towards a horizontal shape (Fig. 1c). An increase in the injection of hot

holes and enhanced hot-cold interactions is then expected, which consequently lead to an increase in cold holes occupying higher energy states. This explains the distribution peak at -0.12 V. When the bias is further increased, the electric field is distributed uniformly throughout the structure. [25] The lowering of the constant barrier by the image-force effect [15] will facilitate the escape of higher-energy cold holes over the barrier, which leads to another distribution peak at higher negative bias (-0.40 V).

The dynamics of the hot-cold hole interaction is also supported by studies using picosecond infrared spectroscopy. [26,27] It was shown that the carrier-phonon coupling plays an important role in the intervalence-band transitions. [28] Photoexcited holes in the light-hole band or spin-orbit split-off band initially relax, mainly through the emission of optical phonons, typically within a sub-picosecond timescale. The subsequent relaxation proceeds through the dominant hole-hole scattering mechanism, which causes a redistribution of energies among the hot and cold holes. [5] As a consequence, they reach a thermalized state at much higher energies compared to their original states; further relaxation then typically takes relatively long times (tens of picoseconds). [26,27] These "hot" holes are thus able to be excited by absorbing VLWIR photons and escape over the barriers, contributing to the photocurrent. This mechanism is believed to be the main cause of the VLWIR response. To verify such a photoresponse picture, we employ an escape-cone model [29] (see Supplementary Information II) to simulate the response spectra. In this model, free-carrier absorption described by the Drude theory [20] is used to produce the general spectral profile. The threshold energy, which is a fitting parameter in the simulation, determines the long-wavelength end of the response. Using a value of 0.012 eV, the modeled response is in general agreement with

the experiment as shown in Fig. 1d. However, a sharp peak appears at 25.3 μm (or 395 cm^{-1}) which becomes stronger as the bias is increased (Supplementary Information II). Another peak at 35.6 μm (or 281 cm^{-1}) also appears at -0.08 V and sharply increases with negative bias. It was found that these two peaks are close to the two plasmon-phonon coupling modes calculated for the equilibrium (Supplementary Information II), i.e., 23 and 42 μm (or 430 and 236 cm^{-1}) for a doping concentration of $p = 1 \times 10^{19}$ cm^{-3}. The injection of hot holes is expected to disturb the distribution of cold holes by exciting some of the cold holes up to higher-energy states, which should affect the coupling, as it is different from the equilibrium. Despite this hot-hole effect, comparison between the two sharp response peaks and the coupling modes shows the important role of the phonon-plasmon coupling in modifying the response. In addition to this, the general spectral profile of the VLWIR response agrees with the escape-cone model; in particular, features associated with GaAs and AlAs-like phonons are well explained.

It may be noted that observing a positive-bias hole distribution peak [at 0.10 V; see Fig. 2c] is uncommon. A possible reason is the non-linear increase of photocurrent with bias due to the asymmetric band alignment. Nevertheless, the negative-bias condition leads to the optimum VLWIR response, which is much stronger than that under positive bias, consistent with observations from hot-carrier spectroscopy. [23,24,30]

Hot-hole induced photoresponse and its tailorability

The proposed mechanism for the hot-hole response implies a need for injecting hot holes to trigger the VLWIR response. This can be achieved through electrical and/or optical approaches. For the electrical approach, to obtain a non-trivial current passing through the graded barrier, a bias substantially higher than that at which hole distribution peaks are observed, is required. Under such a high bias, the VLWIR response is no longer present. An optimized solution is to separate the injection of hot holes [23,24] and the collection of photoexcited holes by altering the device structure. Here, we show the optical approach; the advantage of this is that it gives a convenient control of the hot-hole injection through varying the optical intensity. Figure 3a shows a schematic diagram of the experimental apparatus. A cut-on wavelength (λ_{CO}) is selected, and a long-pass filter is used to block high-energy photons from the FTIR spectrometer from being incident onto the sample. Figures 3b – 3d map the SW, which is measured using filters with different λ_{CO} (the GaAs beamsplitter and optical excitation source are not used in this case). Increasing λ_{CO} reduces the energies of the injected hot holes, thus reducing the VLWIR response. The use of $\lambda_{\mathrm{CO}} = 4.5$ μm (Fig. 3d) fully suppresses the VLWIR response because of the absence of hot holes in the absorber. However, as shown in Fig. 3e, the VLWIR response can be recovered by utilizing an optical excitation source which induces hot hole injection. These results are in good agreement with the hot-cold hole energy transfer mechanism.

To show the tunability of the VLWIR response, we carried out a further detailed set of measurements using the optical excitation source (Fig. 3a). A $\lambda_{\mathrm{CO}} = 4.5$ μm long-pass filter is used

throughout so that light from the FTIR spectrometer solely acts as a probe to detect the spectral response. The map of SW at different excitation levels are shown in Fig. 4a, with Fig. 4b showing the excitation power spectra which were tailored by a short-pass filter (quartz glass, up to $\sim$ 4.8 μm). The variation of the VLWIR response (at -0.1 V) with the excitation power is plotted in Figs. 4c and 4d, showing features associated with the cut-on wavelength of the filter and the $2 \times$ TO(X) phonons of the GaAs beamsplitter. [31] These results demonstrate the dominant dependence of the VLWIR response on the excitation intensity. By increasing the excitation intensity, one may expect to tune the energies of cold holes and thus reduce the threshold energy of the VLWIR response from 0.32 eV (the original value of cold holes) to 0 eV. However, such a characteristic was not identified experimentally. We also tried very weak excitation which leads to a weak VLWIR response, but its threshold stays nearly the same. This leads us to conclude that the dominant hot-cold hole interaction and the energy transfer process take place through single hole-hole scattering events, rather than multiple scattering. As a consequence, cold holes are excited into states with nearly the same energies, despite the intensity of the pump light incident onto the sample; this process is independent of their original states and the absorber thickness. Notice that samples SP1005 – 1007 display similar spectral shape (Fig. 1e). This also accounts for why the strength of the VLWIR response, instead of its threshold, varies with the excitation level.

In view of the lack of VLWIR response in a symmetric flat-barrier sample (LH1002), the barrier offset between the two barriers (lying above and below the absorber) plays an important role in triggering the VLWIR response (Supplementary Information II). Such an offset causes the energies of holes to be higher on the injection side compared with the collection side [Fig. 1c]. [12]

The threshold energy (0.012 eV) obtained from the escape-cone model simulation indicates that cold holes remain very close to the band edge of the barrier. This can be understood in terms of energy transfer through single hole-hole scattering. To obtain a response at a photon energy of 0.012 eV, the energy passed from a hot hole to a cold hole is about 0.27 eV (to excite a cold hole near the Fermi level), which is less than the total excess energy of the hot hole (about 0.38 eV relative to the Fermi level). Notice that this result allows us to exclude band filling effects as a cause of the VLWIR response, as a large number of holes would be needed to fill up energy states spanning an energy range of 0.27 eV, which is impossible under our experimental conditions. Also, since a higher capture probability is expected in the flat-barrier structure compared to the graded-barrier structure, a band filling effect would be expected to lead to higher VLWIR response in sample LH1002, which is opposite to our observations. A small value of the threshold energy (e.g., 0.012 eV as simulated) will facilitate operation at a low bias and suppress the current component associated with hot holes $-$ the hot-hole current increase with bias can overwhelm the VLWIR radiation caused photocurrent at higher biases.

The responsivity of our samples is of the order of 10 $\mu\mathrm{A/W}$, which is relatively low compared to reported detectors. [17] The use of a single-emitter structure with relatively low absorption is one of the reasons. Also, the bulk semiconductor based absorber leads to a fast carrier lifetime (e.g., ~ 0.1 ps for $p = 1 \times 10^{19}$ cm^{-3}). By using structures such as quantum dots, an increase in the lifetime by a factor of 10^4–10^8 is possible. [32] Despite the low responsivity, an advantage of our results is the negligible dark current owing to the high activation energy (0.32 eV), even though a VLWIR response is obtained. This offers the possibility of incorporating a long-wavelength re-

sponse into a short-wavelength detector. In fact, the noise current is far below the experimental sensitivity ($\sim 10^{-15}$ A/Hz$^{1/2}$). Using this limit, a conservative estimate of the specific detectivity is $\sim 1 \times 10^9$ cm·Hz$^{1/2}$/W (using the highest responsivity of up to 69 $\mu\mathrm{A/W}$; see Supplementary Information II). In addition to the 5.3 K operation, we have measured the VLWIR response up to 30 K, showing the possibility of higher-temperature operation (Supplementary Information II). Optimized quantum structures may lead to improvement in the responsivity as well as the operating temperature.

The use of an external optical excitation source provides an optimized solution for realizing a VLWIR detector, for example, integrating a VLWIR detector with a light-emitting diode (LED); the resultant device will be compact, and can be monolithically grown by traditional growth methods. The device scheme is similar to the reported up-converter [33] (Fig. 4e), where the output of a photodetector upon absorbing infrared radiation drives a LED to emit visible light. In contrast to this, the hot-carrier detector utilizes emission from the LED to initiate the injection of hot carriers and triggers the VLWIR response, in analogy to the experiment shown in Figs. 4a – 4d. Despite a more "compact" realization being possible, we note that we have demonstrated the discovery of a new hot-hole principle, which is capable of surpassing the conventional spectral limit of current optoelectronic devices.

Conclusion

Our findings open up many possibilities for new applications based on traditional semiconductor technologies, for example, utilizing well established III-V semiconductor epitaxy and process technology. Normally, applications of semiconductors are confined to specific wavelength ranges in accordance with their band gaps. [34] With the additional degree of freedom enabled by tuning the energies of cold carriers, it is now possible for a particular material to respond beyond its standard spectral limit. In addition to photodetection, the hot-carrier concept can be applied to photovoltaic devices, which, in addition to their original absorption band, will have wavelength-extended absorbing capabilities, with a tunability controlled through varying the degree of hot-hole injection in order to meet the demands of specific applications. Moreover, the hot-carrier effect is expected to improve energy efficiency of both photodetectors and photovoltaics, since the energies of hot carriers are diverted from heating the lattice to heating cold carriers.

Methods

Device structure. The active regions of samples SP1005 – 1007 consist of (from top to bottom) a 400 nm-thick undoped $Al_{0.57}Ga_{0.43}As$ constant barrier, a p-type GaAs layer (absorber) ($p = 1 \times 10^{19}$ cm^{-3}), and an 80 nm-thick $Al_xGa_{1-x}As$ graded barrier with x linearly varying from 0.75 (top) to 0.45 (bottom). The thicknesses of the p-type GaAs absorbers are 20 nm, 50 nm and 80 nm for SP1005, 1006, 1007, respectively. The absorber of sample LH1002 is 18.8 nm-thick p-type ($p = 1 \times 10^{19}$ cm^{-3}) GaAs, which is placed between $Al_xGa_{1-x}As$ barriers with the same Al fraction ($x = 0.57$) and thickness (60 nm). All active regions are sandwiched between two

p-type ($p = 1 \times 10^{19}$ cm^{-3}) GaAs ohmic contact layers. The activation energy (Δ) is associated with the p-type GaAs/Al$_x$Ga$_{1-x}$As junction, defined as the energy difference between the Fermi level of p-type GaAs and Al$_x$Ga$_{1-x}$As barrier (valence-band edge). It is calculated to be 0.25 eV, 0.32 eV and 0.42 eV for barriers with Al fractions of 0.45, 0.57 and 0.75, respectively, by taking into account band offsets at the heterointerface and doping-induced band gap narrowing.

Fabrication. Detectors were processed by wet etching to produce square mesas, which was followed by evaporation of Ti/Pt/Au ohmic contacts onto the top and bottom p-type GaAs contact layers. A top ring contact with a window opened in the center was fabricated to allow front-side illumination. The experiments were carried out on 400×400 μm^2 mesas with an open area of 260×260 μm^2.

Characterization. The dark current-voltage-temperature characteristics were measured by mounting the sample in a variable temperature cryostat, and using a Keithley 2400 Source Meter and a computer controlled Keithley Switch System for selecting different mesas. For photoresponse measurements, samples were mounted in a liquid-helium dewar, and measured by using a Perkin-Elmer system 2000 FTIR spectrometer. The sample acts as a custom detector in place of the built-in detector of the spectrometer. The photovoltage signal from the sample upon light illumination is amplified by a low-noise preamplifier (Stanford Research Systems SR560) and feeds into the spectrometer. The spectral range of photoresponse covers a broad wavelength range from 1.5 to 55 μm, which consists of two working ranges of the beam splitters for the FTIR spectrometer. KBr and 6-μm Mylar beam splitters were used to measure the wavelength ranges of 1.5 – 23 μm and 23 – 55 μm, respectively.

Acknowledgements This work was supported in part by the US Army Research Office under Grant No. W911NF-12-2-0035 monitored by William W. Clark, and in part by the U.S. National Science Foundation under Grant No. ECCS-1232184. The University of Leeds acknowledges supports from the UK Engineering and Physical Sciences Research Council, and EHL from the European Research Council Advanced Grant "TOSCA". HCL acknowledge support from the National Major Basic Research Projects (2011CB925603) and the Natural Science Foundation of China (91221201 and 61234005).

Author contributions A.G.U.P. conceived the split-off heterojunction concept and was involved in designing the device structure. Y.F.L. and A.G.U.P. conceived the experiments and wrote the paper. L.H.Li, S.P.K. and E.H.L. grew the samples using molecular beam epitaxy. H.C.L. carried out the device processing. Y.F.L. performed electrical and optical measurements, and data analysis. A.G.U.P. guided this project. All authors contributed to the content in the paper.

Additional information The authors declare no competing financial interests. Supplementary information accompanies this paper at www.nature.com/naturephotonics. Correspondence and requests for materials should be addressed to A.G.U.P. (email: uperera@gsu.edu).

References

1. Freitag, M., Low, T., Xia, F. & Avouris, P. Photoconductivity of biased graphene. *Nature Photonics* **7**, 53–59 (2013).

2. Gabor, N. M. *et al.* Hot carrier-assisted intrinsic photoresponse in graphene. *Science* **334**, 648–652 (2011).

3. Sun, Z. *et al.* Infrared photodetectors based on CVD-grown graphene and PbS quantum dots with ultrahigh responsivity. *Advanced Materials* **24**, 5878–5883 (2012).

4. Yan, J. *et al.* Dual-gated bilayer graphene hot-electron bolometer. *Nature Nanotechnology* **7**, 472–478 (2012).

5. Rossi, F. & Kuhn, T. Theory of ultrafast phenomena in photoexcited semiconductors. *Rev. Mod. Phys.* **74**, 895–950 (2002).

6. Winnerl, S. *et al.* Carrier relaxation in epitaxial graphene photoexcited near the dirac point. *Phys. Rev. Lett.* **107**, 237401 (2011).

7. Rosenwaks, Y. *et al.* Hot-carrier cooling in GaAs: quantum wells versus bulk. *Phys. Rev. B* **48**, 14675–14678 (1993).

8. Jalabert, R. & Das Sarma, S. Inelastic scattering in a doped polar semiconductor. *Phys. Rev. B* **41**, 3651–3654 (1990).

9. Petersen, C. L. & Lyon, S. A. Observation of hot-electron energy loss through the emission of phonon-plasmon coupled modes in GaAs. *Phys. Rev. Lett.* **65**, 760–763 (1990).

10. Sicault, D., Teissier, R., Pardo, F., Pelouard, J.-L. & Mollot, F. Experimental study of hot-electron inelastic scattering rate in p-type InGaAs. *Phys. Rev. B* **65**, 121301 (2002).

11. Xiao, J. *et al.* Carrier multiplication in semiconductor nanocrystals detected by energy transfer to organic dye molecules. *Nature Communications* **3**, 1170 (2012).

12. Capasso, F. Band-gap engineering: from physics and materials to new semiconductor devices. *Science* **235**, 172–176 (1987).

13. Kang, Y. *et al.* Monolithic germanium/silicon avalanche photodiodes with 340 GHz gain-bandwidth product. *Nature Photonics* **3**, 59–63 (2009).

14. Sze, S. M. & Ng, K. K. *Physics of Semiconductor Devices* (John Wiley & Sons, New York, 2007).

15. Lao, Y.-F. & Perera, A. G. U. Temperature-dependent internal photoemission probe for band parameters. *Phys. Rev. B* **86**, 195315 (2012).

16. Rinzan, M. B. M. *et al.* AlGaAs emitter/GaAs barrier terahertz detector with a 2.3 THz threshold. *Appl. Phys. Lett.* **86**, 071112 (2005).

17. Perera, A. G. U. *et al.* GaAs multilayer p^+-i homojunction far-infrared detectors. *J. Appl. Phys.* **81**, 3316–3319 (1997).

18. Matsik, S. G. *et al.* Cutoff tailorability of heterojunction terahertz detectors. *Appl. Phys. Lett.* **82**, 139–141 (2003).

19. Chapler, B. C. *et al.* Infrared probe of the insulator-to-metal transition in $Ga_{1-x}Mn_xAs$ and $Ga_{1-x}Be_xAs$. *Phys. Rev. B* **84**, 081203 (2011).

20. Lao, Y.-F. & Perera, A. G. U. Dielectric function model for p-type semiconductor inter-valence band transitions. *J. Appl. Phys.* **109**, 103528 (2011).

21. Newman, R. & Tyler, W. W. Effect of impurities on free-hole infrared absorption in p-type germanium. *Phys. Rev.* **105**, 885–886 (1957).

22. Schneider, H. & Liu, H. C. *Quantum Well Infrared Photodetectors: Physics and Applications*, vol. 126 of *Springer series in optical sciences* (Springer, New York, 2007).

23. Hayes, J. R., Levi, A. F. J. & Wiegmann, W. Hot-Electron Spectroscopy of GaAs. *Phys. Rev. Lett.* **54**, 1570–1572 (1985).

24. Levi, A. F. J., Hayes, J. R., Platzman, P. M. & Wiegmann, W. Injected-hot-electron transport in GaAs. *Phys. Rev. Lett.* **55**, 2071–2073 (1985).

25. Thibaudeau, L., Bois, P. & Duboz, J. Y. A self-consistent model for quantum well infrared photodetectors. *J. Appl. Phys.* **79**, 446–454 (1996).

26. Woerner, M., Elsaesser, T. & Kaiser, W. Relaxation processes of hot holes in *p*-type germanium studied by picosecond infrared spectroscopy. *Phys. Rev. B* **45**, 8378–8387 (1992).

27. Elsaesser, T. *et al.* Relaxation processes of hot holes in Ge and GaAs investigated by ultrafast infrared spectroscopy. *Semicond. Sci. Technol.* **9**, 689 (1994).

28. Lao, Y.-F. *et al.* Direct observation of spin-orbit splitting and phonon-assisted optical transitions in the valence band by internal photoemission spectroscopy. *Phys. Rev. B* **88**, 201302 (2013).

29. Esaev, D. G., Rinzan, M. B. M., Matsik, S. G. & Perera, A. G. U. Design and optimization of GaAs/AlGaAs heterojunction infrared detectors. *J. Appl. Phys.* **96**, 4588–4597 (2004).

30. Brill, B. & Heiblum, M. Electron heating in GaAs due to electron-electron interactions. *Phys. Rev. B* **49**, 14762–14765 (1994).

31. Blakemore, J. S. Semiconducting and other major properties of gallium arsenide. *J. Appl. Phys.* **53**, R123 (1982).

32. Matthews, M. R. *et al.* Transient photoconductivity measurements of carrier lifetimes in an InAs/$In_{0.15}Ga_{0.85}As$ dots-in-a-well detector. *Appl. Phys. Lett.* **90**, 103519 (2007).

33. Chen, J. *et al.* Hybrid organic/inorganic optical up-converter for pixel-less near-infrared imaging. *Advanced Materials* **24**, 3138–3142 (2012).

34. Sang, L., Hu, J., Zou, R., Koide, Y. & Liao, M. Arbitrary multicolor photodetection by hetero-integrated semiconductor nanostructures. *Scientific Reports* **3**, 1 (2013).

Figure captions

Figure 1 Sample structure and the VLWIR response at 5.3 K. a, Schematic diagram of the p-type GaAs/$Al_xGa_{1-x}As$ structures. **b,** Calculated equilibrium valence-band alignment, with and without image-force barrier lowering [15] (thick-gray and dashed-blue lines, respectively). **c,** Schematic valence band diagrams (including band bending) under negative bias (positive polarity applied on the injector), with a comparison of hole photoexcitation and emission without (top) and with (bottom) the hot-cold hole energy transfer. **d,** Photoresponse at 5.3 K. The dashed line is the escape-cone model fit. The marked features are associated with GaAs and AlAs-like phonons. **e,** Comparison of the response for samples SP1005 – 1007 and LH1002 at 5.3 K. The optical power spectrum of the FTIR spectrometer used in the experiment (incident on a sample with active area of 260×260 μm^2) is also shown.

Figure 2 Spectral weight (SW) of response and differential photocurrents. a, The variation of SW (sample SP1007) with bias and λ_{min}, calculated using Eq. 1 where λ_{max} is 55 μm. **b,** Bias-dependent SW. Values used for λ_{max} determine SW^{tot} and SW^{pump}. SW^{tot} corresponds to all of the holes being collected. SW^{pump} is calculated by using $\lambda_{max} = 2.95$ μm (i.e., 0.42 eV, the maximum of the graded barrier). SW^{tot} displays two maxima compared to SW^{pump}, due to the bias-dependent VLWIR response. **c,** Differential SW^{pump} (proportional to I_{ph}^{pump}) (top) and differential photocurrents measured using different optical excitation sources (bottom).

Figure 3 Photoresponse obtained using long-pass filters and an external optical excitation source. a, Experimental apparatus, where the semi-insulating GaAs is double-side polished and acts as a beamsplitter. **b – d,** Spectral weights (SW) of the response (sample SP1007) measured by using long-pass filters with cut-on wavelengths ($\lambda_{\rm CO}$) of **b,** 2.4 μm, **c,** 3.6 μm and **d,** 4.5 μm, respectively. The VLWIR response is graduallly diminished by increasing $\lambda_{\rm CO}$, and is barely seen when a $\lambda_{\rm CO} = 4.5$ μm filter is used. **e,** Recovery of the VLWIR response by providing hot holes through an external optical excitation source, measured with a 4.5 μm long-pass filter.

Figure 4 Tuning the VLWIR response. a, Spectral weights (SW) of response at different excitation levels through controlling the power of an optical source (see Fig. 3a for the experimental apparatus). The experiment was carried out on sample SP1006, which has a very similar VLWIR response to SP1007. **b,** Power spectra of the optical source (incident on the sample with an active area of 260×260 μm^2). A quartz glass filter is used to block the long-wavelength portion (up to 4.8 μm). **c – d,** The dependence of the VLWIR response (at -0.1 V) on the excitation power. Indicated by arrows are the cut-on wavelength of the filter and the $2 \times$ TO(X) phonon feature of the GaAs beamsplitter [31], respectively. **e,** Comparison of the up-converter [33] and proposed hot-carrier photodetector.

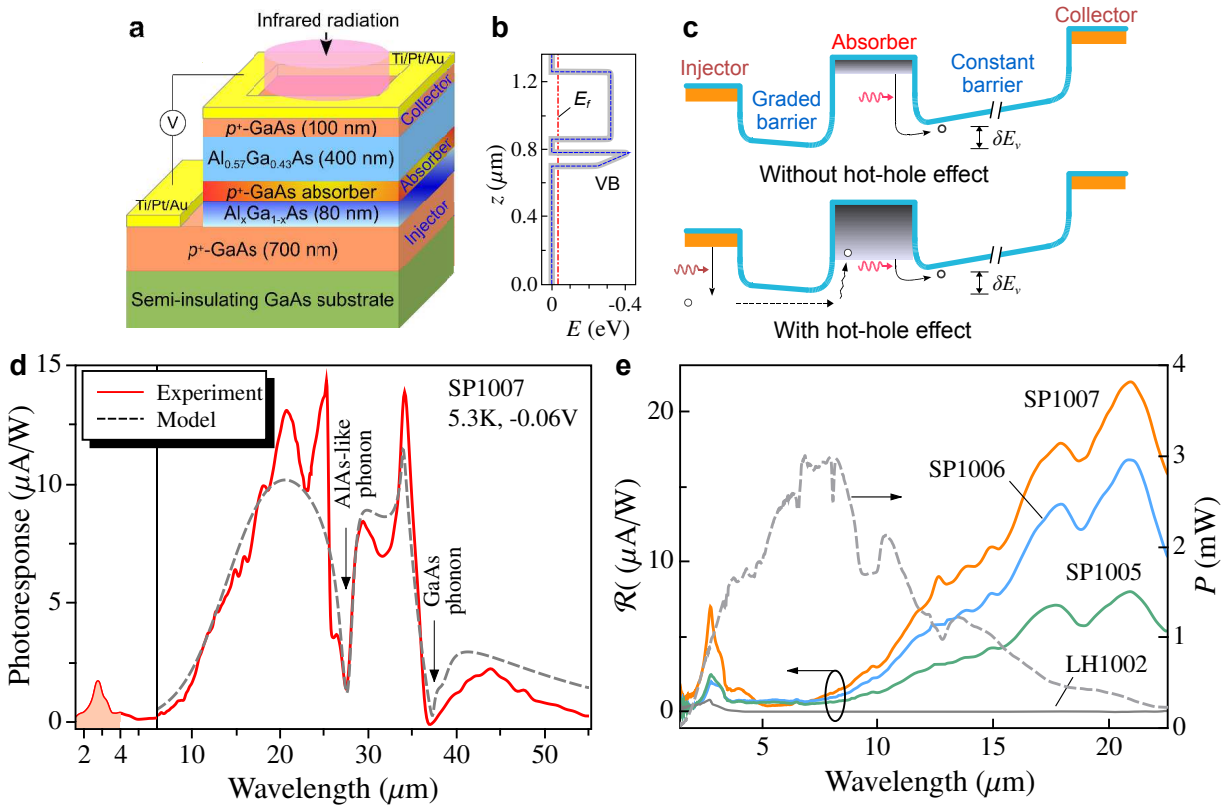
a
Infrared radiation
Ti/Pt/Au
p+-GaAs (100 nm)
Al0.57Ga0.43As (400 nm)
p+-GaAs absorber
AlxGa1-xAs (80 nm)
p+-GaAs (700 nm)
Semi-insulating GaAs substrate
Collector
Absorber
Injector
V
b
z (μm)
E (eV)
Ef
VB
c
Injector
Graded barrier
Absorber
Constant barrier
Collector
δEv
Without hot-hole effect
With hot-hole effect
d
Experiment
Model
SP1007
5.3K, -0.06V
AlAs-like phonon
GaAs phonon
Photoresponse (μA/W)
Wavelength (μm)
e
SP1007
SP1006
SP1005
LH1002
ℛ(μA/W)
P (mW)
Wavelength (μm)

FIG. 1.

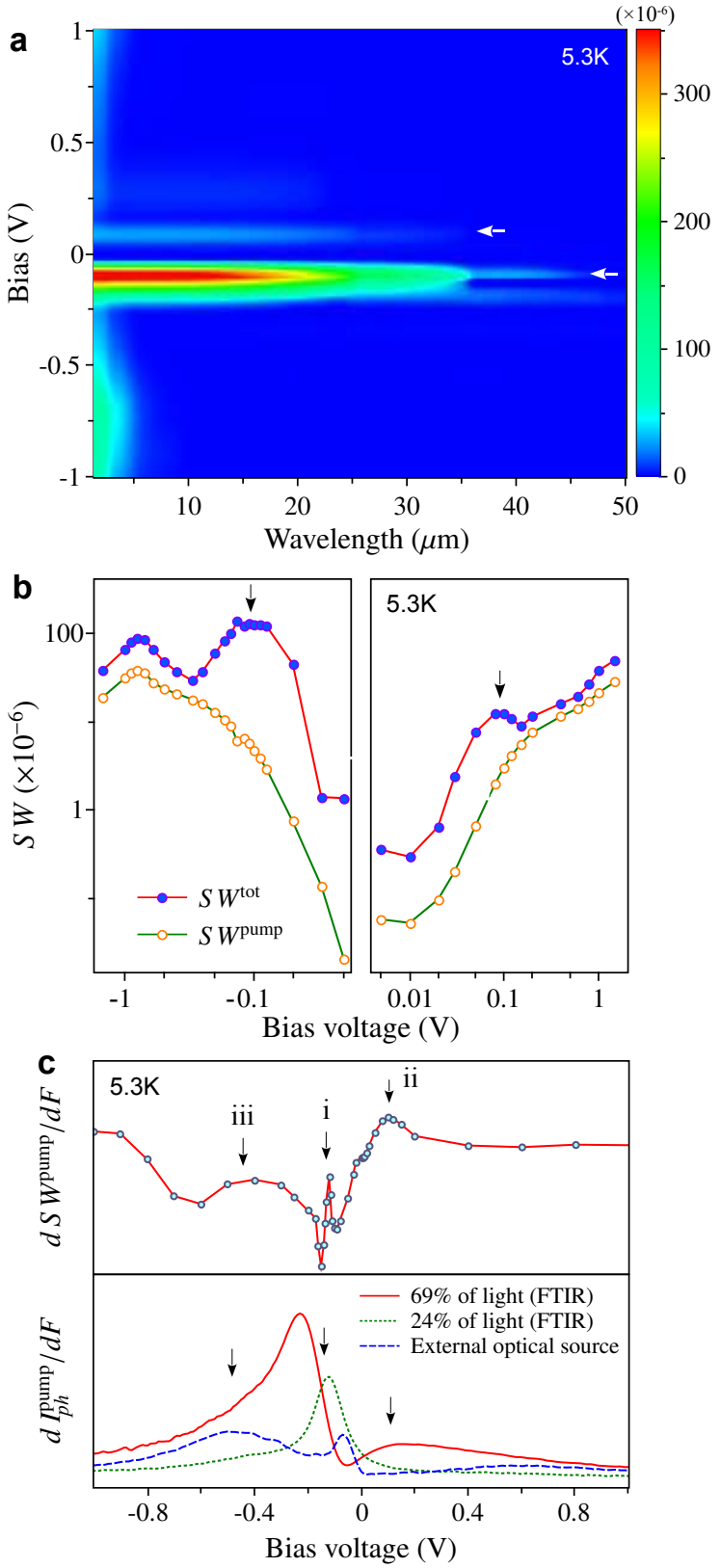
a
5.3K
(×10⁻⁶)
300
200
100
0
1
0.5
0
-0.5
-1
Bias (V)
10
20
30
40
50
Wavelength (μm)
b
5.3K
100
1
SW (×10⁻⁶)
SW^tot
SW^pump
-1
-0.1
0.01
0.1
1
Bias voltage (V)
c
5.3K
iii
i
ii
dSW^pump/dF
69% of light (FTIR)
24% of light (FTIR)
External optical source
dI_ph^pump/dF
-0.8
-0.4
0
0.4
0.8
Bias voltage (V)

FIG. 2.

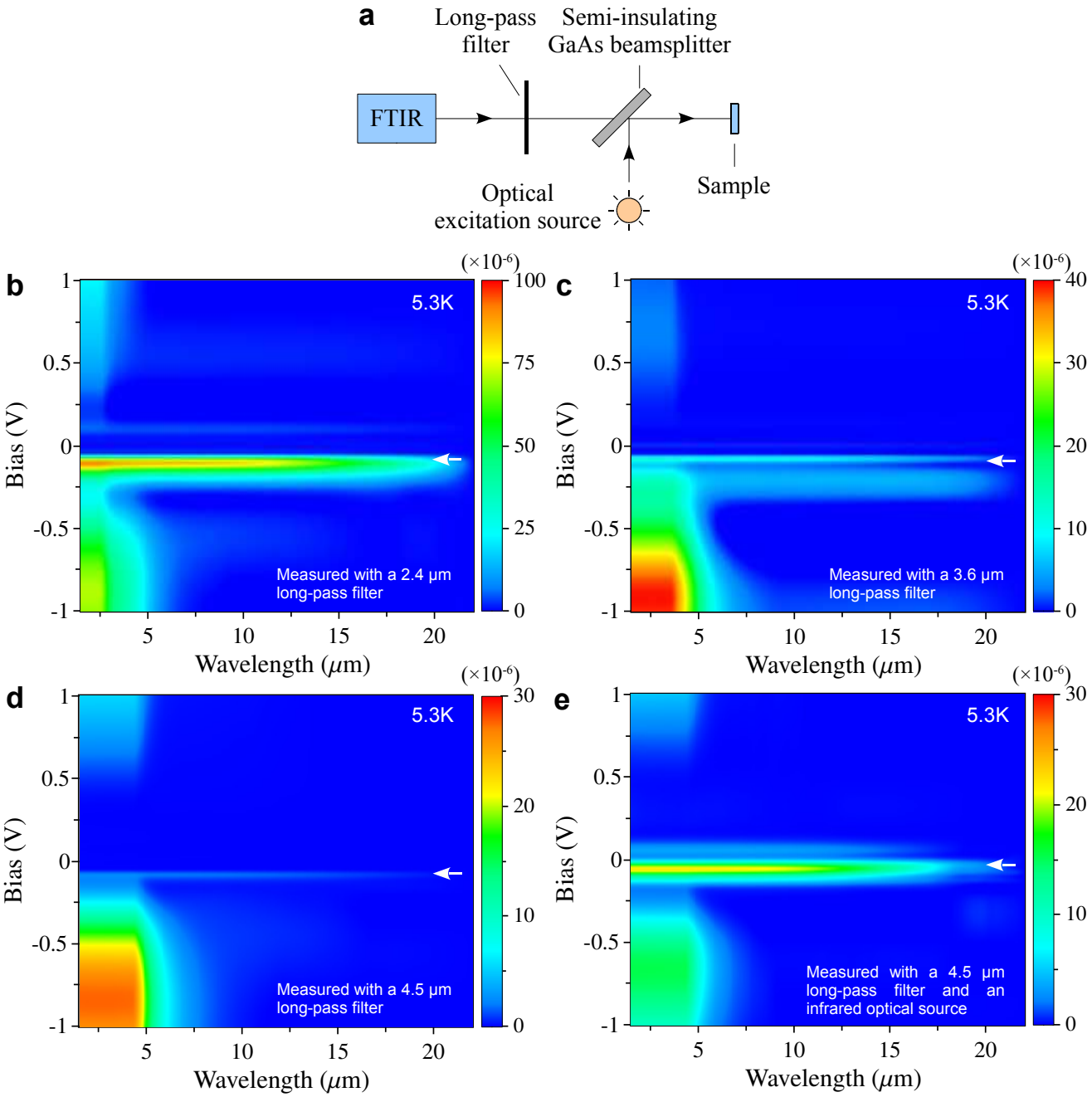
a
Long-pass filter
Semi-insulating GaAs beamsplitter
FTIR
Optical excitation source
Sample
b
5.3K
Measured with a 2.4 μm long-pass filter
c
5.3K
Measured with a 3.6 μm long-pass filter
d
5.3K
Measured with a 4.5 μm long-pass filter
e
5.3K
Measured with a 4.5 μm long-pass filter and an infrared optical source
Bias (V)
Wavelength (μm)
(×10⁻⁶)

FIG. 3.

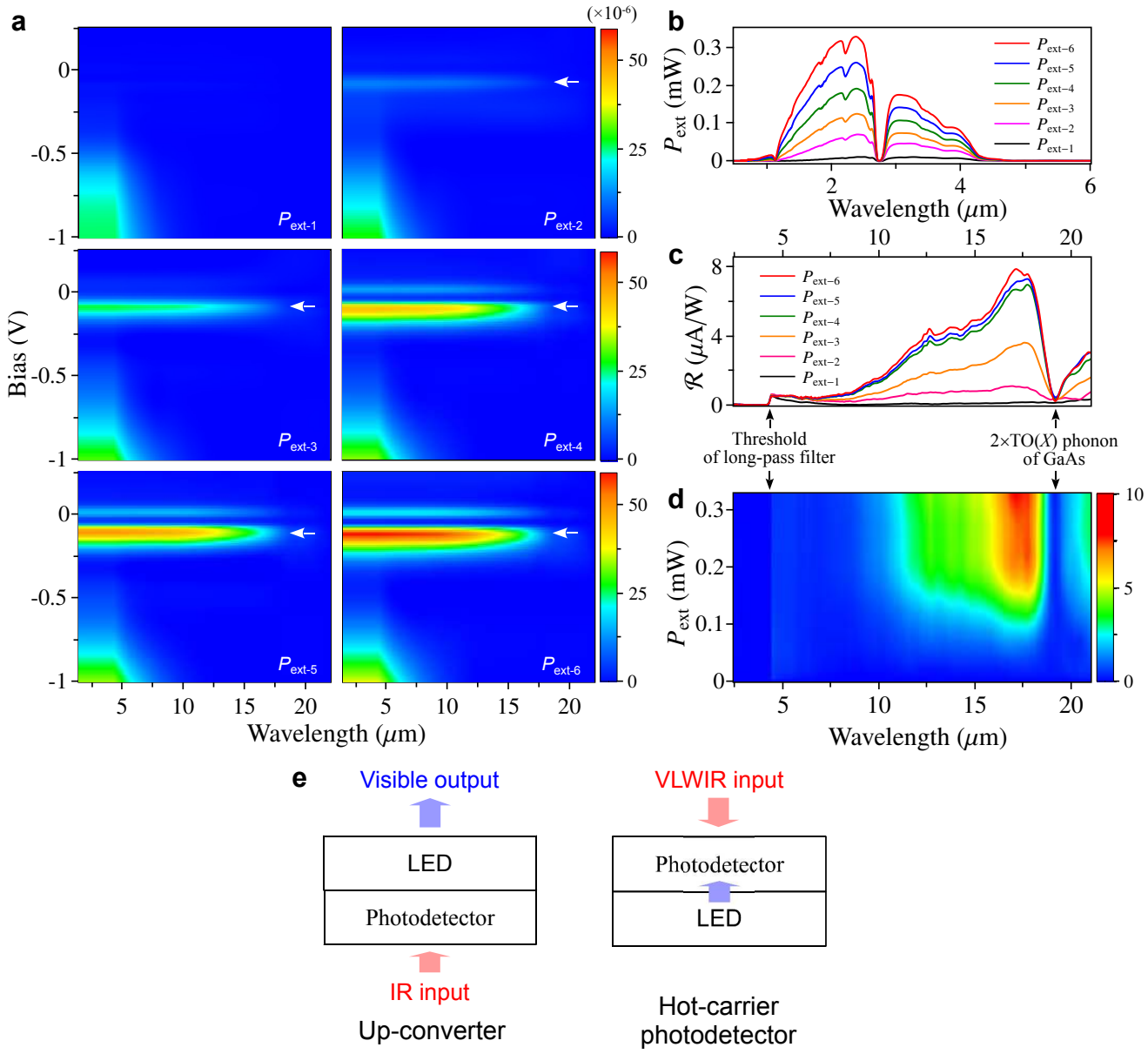
a
b
c
d
e
(×10⁻⁶)
Bias (V)
Wavelength (μm)
P_ext-1
P_ext-2
P_ext-3
P_ext-4
P_ext-5
P_ext-6
P_ext (mW)
ℛ (μA/W)
P_ext−6
P_ext−5
P_ext−4
P_ext−3
P_ext−2
P_ext−1
Threshold
of long-pass filter
2×TO(X) phonon
of GaAs
Visible output
VLWIR input
LED
Photodetector
IR input
Up-converter
Hot-carrier
photodetector

FIG. 4.